



Journal of Mining and Environment (JME)  
journal homepage: [www.jme.shahroodut.ac.ir](http://www.jme.shahroodut.ac.ir)



## Influence of Single Tunnel and Twin Tunnel on Collapse Pattern and Maximum Ground Movement

Vahab Sarfarazi<sup>1\*</sup>, Kaveh Asgari<sup>2</sup>

1- Department of Mining Engineering, Hamedan University of Technology, Hamedan, Iran

2- Department of Mining Engineering, Shahid Bahonar University of Kerman, Kerman, Iran

### Article Info

Received 11 August 2021

Received in Revised form 1  
September 2021

Accepted 7 September 2021

Published online 7 September  
2021

DOI: [10.22044/jme.2021.11088.2085](https://doi.org/10.22044/jme.2021.11088.2085)

### Keywords

Tunnel

PFC2D

Settlement

### Abstract

Particle Flow Code in Two Dimensions (PFC2D) was used in order to examine the influence of single tunnel and twin tunnel on the collapse pattern and maximum ground movement. Since first PFC was calibrated by the experiments, the results obtained were rendered by a uniaxial test. Further, a rectangular model with dimensions of 100 m × 100 m containing both the central tunnel and twin tunnel was built. The center of the single tunnel was placed 25 m under the ground surface, and its diameter changed from 10 m to 35 m with an increment of 5 m. The center of the twin tunnel was situated 25 m under the ground surface, and its diameter was changed from 10 m to 30 m with an increment of 5 m. For measurement of the vertical displacement, one measuring circle with a 2 m diameter was opted on the ground surface above the tunnel roof. The average of the vertical movement of discs covered in these circles was determined as a ground settlement. A confining pressure of 0.01 MPa was applied on the model. The uniaxial compression strength was 0/09 MPa; the results obtained depicted that the tunnel diameter controlled the extension of the collapse zone. Also the vertical displacement at the roof of the tunnel declined by decreasing the tunnel diameter. The ground settlement increased by increasing the tunnel diameter.

### 1. Introduction

In the last decade, in Iran, the construction of various tunnels, especially for the transportation purpose, has been required. In some cases where a tunnel must be built next to another tunnel, the construction process must be carried out in such a way that the existing buildings or sub-surface infrastructure are not endangered or damaged. Thus before the designing level, forecasting the probable interaction impacts is vital. It has been predicted that the surface soil settlements (S) in the presence of a single tunnel under a soft soil follow an inverted Gaussian curve, introduced by Peck [1], and investigated by various researchers and measurements (Mair et al., [2]). The introduced equations are as follow:

$$S = S_{max} \exp\left(\frac{-x^2}{2i^2}\right) \quad (1)$$

$$S_{max} = \frac{V_s}{\sqrt{2\pi i}} = 1.252 \frac{V_L R^2}{i}$$

The perpendicular or normal spacing from the centerline axis of the tunnel is shown by x,  $S_{max}$  is the maximum settlement of the soil surface (upper than the tunnel axis), i is the horizontal settlement,  $V_s$  is the decline of volume,  $V_L$  is the ground loss percentage in the case that soil is uncontactable ( $V_L = V_s/\pi R^2$ ), and R is the radius of the tunnel. Due to the loss in the tunnel, these settlements are developed. It might be distinguished as the further volume of extracted soil over the volume of final lining. In the process of excavation, the excavated soil in the surrounding of tunnel face is unloaded, and moving inward continues. Due to the nature or properties of the tunnel shield, losses may happen behind the tunnel face. Several site investigations

✉ Corresponding author: [vahab.sarfarazi@gmail.com](mailto:vahab.sarfarazi@gmail.com) (V. Sarfarazi).

have proved that Equation 1 is compatible with the green-field sites (Mair et al., [2]); however, in the presence of buildings in cities, this equation is no longer valid. In the case of the tunnels with multiple installations, each settlement is determined by Equation 1 and accumulated. During the installation or construction of each one, the tunnel interaction has been neglected in this equation. It is obvious that construction of tunnels causes the disturbance of soil, which leads to a change in the soil characteristics or it causes the redistribution of the impact of a later tunneling installation in that area. Due to emplacing the new tunnel, the former one and the surrounding soil transfer like a solid structure. The development of “arching” in the surrounding of the new tunnel occurs as the soil stresses are redistributed, and consequently, a sluggish unloading from the tunnel takes place. When a new tunnel is emplaced in the vicinity of the former tunnel, it leads to the distortion and displacement of the first tunnel lining. Based on the position of the soil and its characteristics, the minimum assumed distinct spacing between the tunnels is determined in order to avoid the interaction impacts. When it comes to multiple tunnels, the superposition procedure is proposed, which is according to the Gauss distribution, as follows (Mair et al., [2]):

$$S = S_{\max(1)} \exp \left[ \frac{(x + \frac{T_s}{2})^2}{2i_{(1)}^2} \right] + S_{\max(2)} \exp \left[ \frac{(x - \frac{T_s}{2})^2}{2i_{(2)}^2} \right] - S_{12} \quad (2)$$

where  $S_{12} = 0$  for the absence of interaction and  $T_s$  is the spacing of the tunnels. In the case of ground loss and the diameters of two tunnels being identical,  $S_{\max(1)} = S_{\max(2)}$  and  $i_{(1)} = i_{(2)}$ . Totally, the settlement of ground is:

$$S = S_{\max} \left\{ \exp \left[ \frac{(x + \frac{T_s}{2})^2}{2i^2} \right] + \exp \left[ \frac{(x - \frac{T_s}{2})^2}{2i^2} \right] \right\} \quad (3)$$

Movements of ground caused by single tunneling have been widely studied by several ways such as field observation (e.g. Peck, [1]; Cording and Hansmire, [3]; analytical approach (e.g. Loganathan and Poulos, [4]; Bobet, [5]), numerical modelling (e.g. Rowe et al., [6]; Addenbrooke [7]; Franzius et al. [8]; Zhao [9]; Jain [10]; Thai [11]; Zhang [12]; Li [13]; Ding [14]; Yang [15]; Zheng [16]; Yang [17]; Zhang [18]; Aalianvari [19]), and physical modelling (e.g. Mair [20]; Taylor [21]). Furthermore, investigations of the ground

movements caused by multiple tunneling have been carried out. Some researchers have shown that the surface settlement troughs are established by twin tunnels with different forms (e.g. Cording and Hansmire [3]; Cooper et al. [22]; Suwansawat and Einstein [23]). In the case of studying the movement associated with multiple tunneling, due to the low-field data investigations generally using numerical modelling (e.g. Addenbrooke [24]; Hunt [25]; Zhou [26]; Zou [27]; Chen [28]; Zhang [29]; Eftekhari [30]; Li [31]; Gao [32]; Li [33]; Sun [34]; Wu [35]; Lee [36]; Wang [37]; Xue [38]; Wang [39,40]) and physical modelling (e.g. Chapman et al. [41,42]; Divall [43]), It is clear that both the numerical and physical modellings give a valuable insight, although due to the intrinsic uncertainties in tunnel engineering, the settlement quantities presented by these investigations can barely represent the real quantities found in an actual condition. In this investigation, the impact of single tunnel and twin tunnel on the collapse pattern and maximum ground movement was examined by Particle Flow Code in Two Dimensions (PFC2D).

## 2. Particle Flow Code

Particle flow code in two dimensions (PFC2D) is a discrete element code that introduces the substance as a rigid particle assembly that can move discretely, and its interaction is just at the contacts (Itasca [44]; Potyondy and Cundall [45]). The same as DEM, a central finite difference method has been used in order to calculate the movements and interaction forces of the particles. Both the linear and non-linear contact models with frictional sliding can be used for the contact models. In this investigation, the linear contact model was used. This model established an elastic relationship between the relative displacements and contact forces of particles. Some provided routines were used in order to produce a parallel-bonded particle model for PFC2D (Itasca [44]). To produce this model, some micro-characteristics must be introduced such as parallel-bond stiffness ratio, minimum radius of ball, stiffness ratio of  $k_n$  over  $k_s$ , ball-to-ball contact modulus, parallel normal bond strength, coefficient of ball friction, ratio of standard deviation to mean of bond strength in both the normal and shear directions, parallel-bond modulus, parallel shear bond strength, and parallel-bond radius multiplier. A calibration approach is critical in order to establish the suitable micro-characteristics used for the assembly of particles. The tests conducted on the laboratory model specimens cannot directly determine the

particle contact and the bonding properties. The characteristics of the materials that are determined by the laboratory tests are macro-mechanical in nature; this is due to the fact that they show a continuum behavior. A reverse modeling approach was applied in order to determine the suitable micro-mechanical characteristics of the numerical models from the macro-mechanical characteristics defined in the laboratory experiments. The trial-and-error method is one of the approaches that is used to connect these two sets of materials property (Itasca [44]). It includes the assumption of the micro-mechanical property values and comparison of the strength and deformation properties of the numerical models with those of the laboratory specimens. The values of micro-mechanical property that generate a simulated macroscopic result close to that of the laboratory tests are then used to assess the ground settlement.

### 2.1. Preparation and calibration of numerical model

The uniaxial compression test and the Brazilian test were applied to calibrate the compressive

strength, young modulus, and tensile strength of the sample in the PFC2D model. The standard process of generation of a PFC2D assembly to show a test model includes four sections: (a) generation and packing of particles, (b) installation of isotropic stress, (c) deletion of floating particle, and (d) bond installation. Using the micro-characteristics listed in Table 1 and the standard calibration approaches (Potyondy and Cundall [45]), a calibrated PFC particle assembly was provided. The dimensions of the uniaxial model were 54 mm and 108 mm. The sample was created by 12,615 particles. The upper and lower walls were moved toward each other with a low velocity of 0.016 m/s. Figure 1a depicts the contact force chain of the numerical tested sample. The contact force chain is like a cone shape. The stress-strain curve is depicted in Figure 1b. This curve is like a typical experimental stress-strain curve in soil. The uniaxial compression strength and the Young modulus were gained by the stress-strain curve (Table 2). These mechanical characteristics were in a good matching with those of the experimental tests (Table 2). This indicates that the calibration of the model is correct.

**Table 1. Micro-characteristics used to introduce the intact rock.**

| Parameter                    | Value | Parameter                                | Value  |
|------------------------------|-------|------------------------------------------|--------|
| Type of particle             | disc  | Stiffness ratio (kn/ks)                  | 2      |
| Density (kg/m <sup>3</sup> ) | 2600  | Particle friction coefficient            | 0.5    |
| Minimum radius (mm)          | 0.27  | Contact bond normal strength, mean (MPa) | 0.002  |
| Size ratio                   | 1.56  | Contact bond normal strength, SD (MPa)   | 0.0004 |
| Porosity ratio               | 0.08  | Contact bond shear strength, mean (MPa)  | 0.002  |
| Damping coefficient          | 0.7   | Contact bond shear strength, SD (MPa)    | 0.0004 |
| Contact young modulus (GPa)  | 1     |                                          |        |

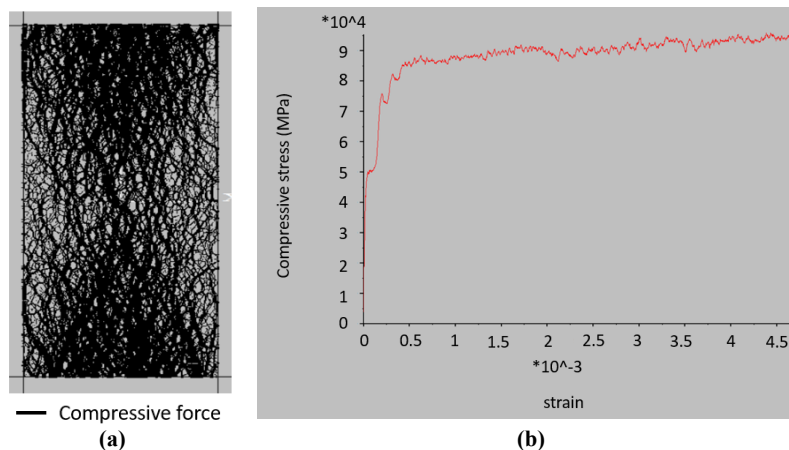


**Figure 1. a) Contact force in numerical model, b) stress-strain curve.**

**Table 2. Brazilian tensile strength of physical and numerical specimens.**

|                                     | Experimental test | Numerical simulation |
|-------------------------------------|-------------------|----------------------|
| Uniaxial compressive strength (MPa) | 0.09              | 0.092                |
| Young modulus (GPa)                 | 0.36              | 0.37                 |

## 2.2. Preparation of model by PFC

After calibration of PFC2D, a rectangular model including a single tunnel and a twin tunnel was built. The dimensions of the rectangular model were 100 m \*100 m. The diameter of a single tunnel was changed from 10 m to 35 m with an increment of 5 m. The center of the single tunnel was situated 25 m under the ground surface (Figure 2). The diameter of the twin tunnel was changed from 10 m to 30 m with an increment of 5 m. The

center of the twin tunnel was situated 25 m under the ground surface (Figure 3). The rectangular model was under a confining pressure of 0.001 MPa. For measurement of the vertical displacement, one measuring circle with a diameter of 2 m was opted on the ground surface above the tunnel roof. The average of the vertical displacement of the discs surrounded in these circles was determined as a ground settlement (Figure 2a and Figure 3a).

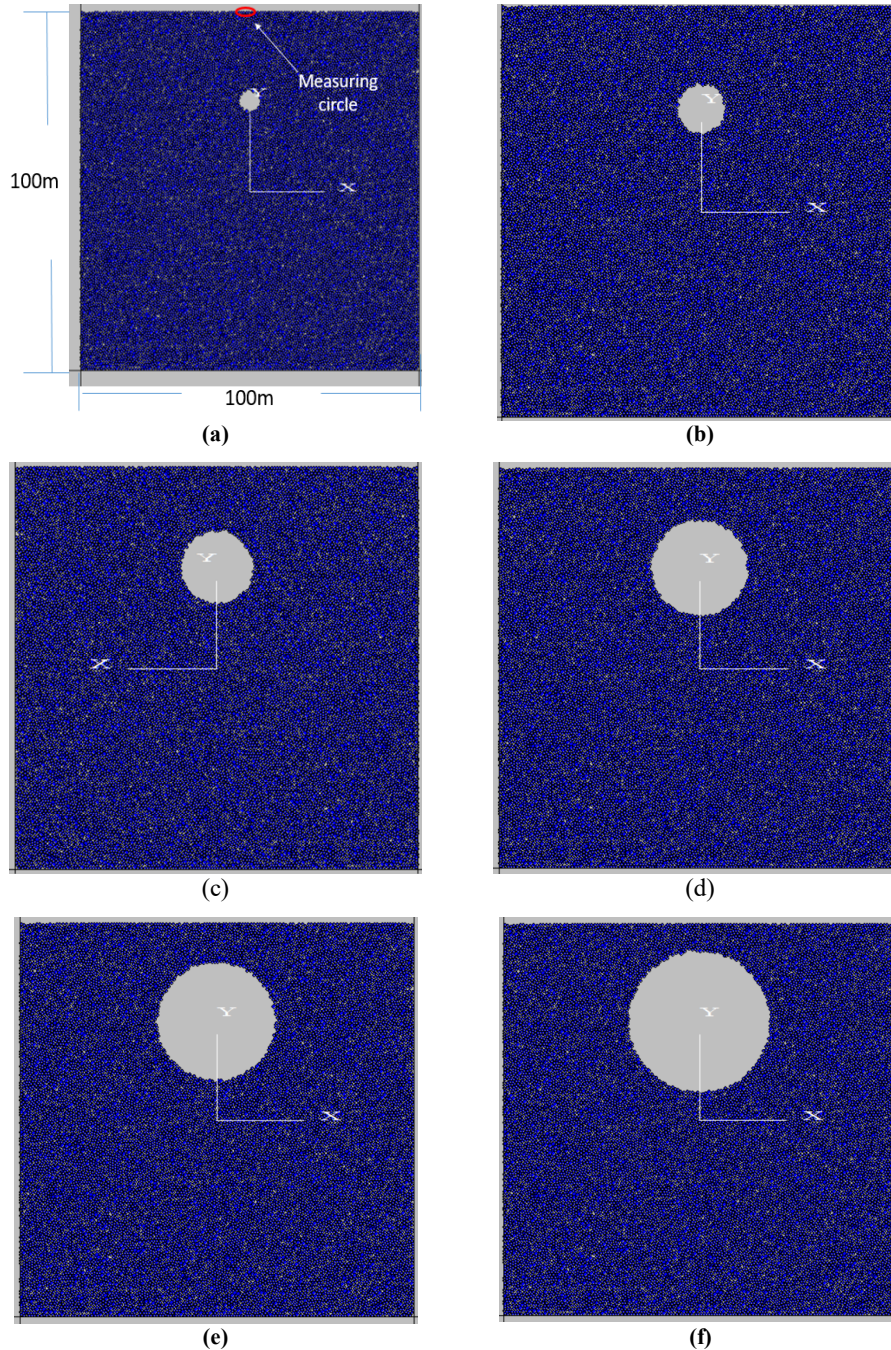


Figure 2. Single tunnel with diameters of a) 10 m, b) 15 m, c) 20 m, d) 25 m, e) 30 m, and f) 35 m.

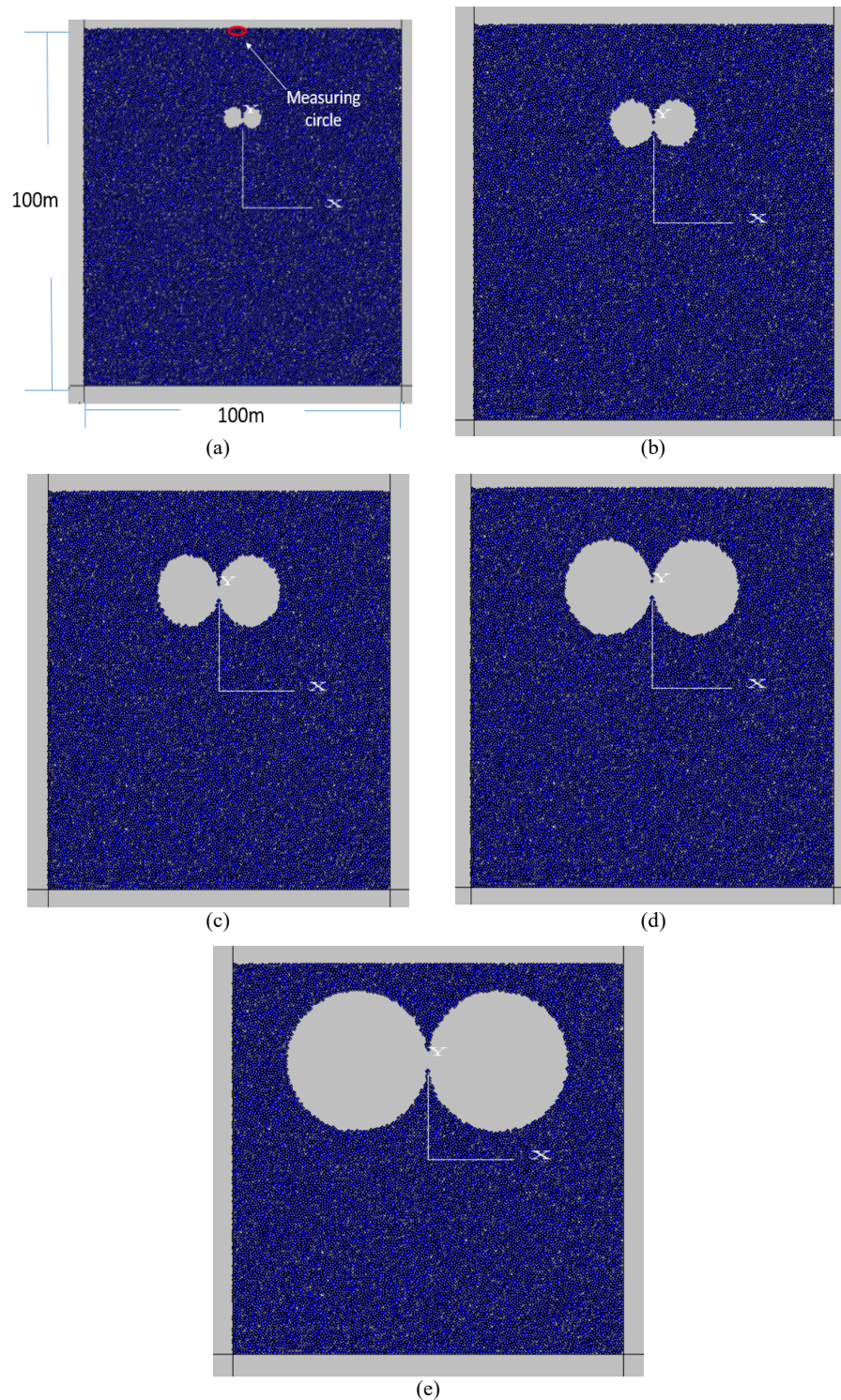


Figure 3. Twin tunnel with diameters of a) 10 m, b) 15 m, c) 20 m, d) 25 m, e) 30 m.

### 3. Numerical results

#### 3.1. Influence of single tunnel on collapse pattern of numerical model

When the diameter of single tunnel was 10 m (Figure 4), a wedge of particles collapsed inside

the tunnel. The size of this wedge was incremented by incrementing the tunnel diameter. The particles of the side-wall of tunnel moved inside the tunnel. It is to be noted that the curvature of the ground surface increase by increasing the tunnel diameter.

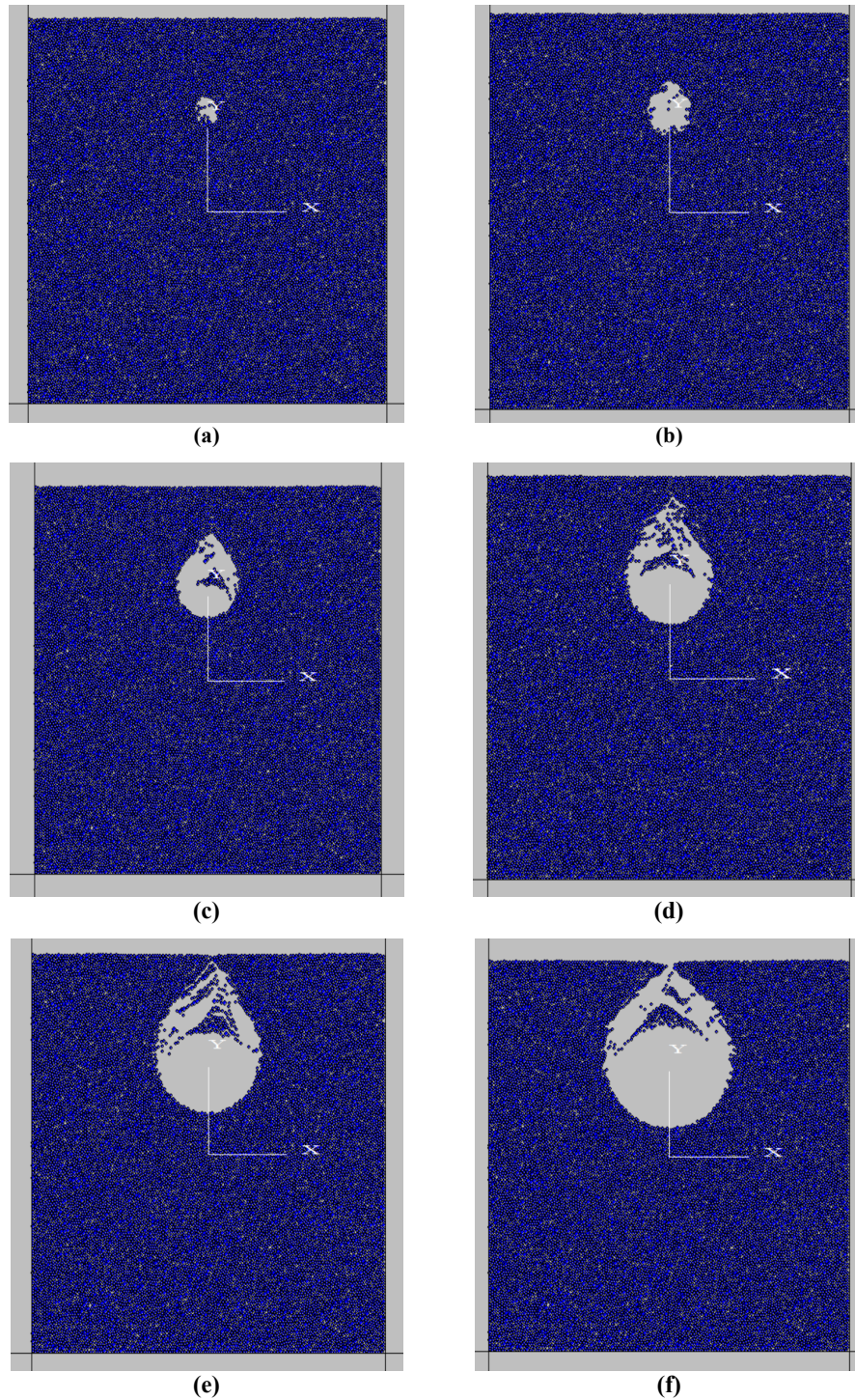


Figure 4. Collapse pattern in single tunnel with diameters of a) 10 m, b) 15 m, c) 20 m, d) 25 m, e) 30 m, and f) 35 m.

### 3.2. Influence of twin tunnel on collapse pattern of numerical model

When the diameter of each tunnel was 10 m (Figure 5), two wedge of particles collapsed inside the tunnel. The size of these wedges was incremented by incrementing the tunnel diameter.

The particles of the side-wall of tunnel moved inside the tunnel. It is to be noted that the curvature of ground surface increase by incrementing the tunnels diameter. By comparing Figure 4 and Figure 5, it can be concluded that the volume of the

collapse zone increase by increasing the tunnel number.

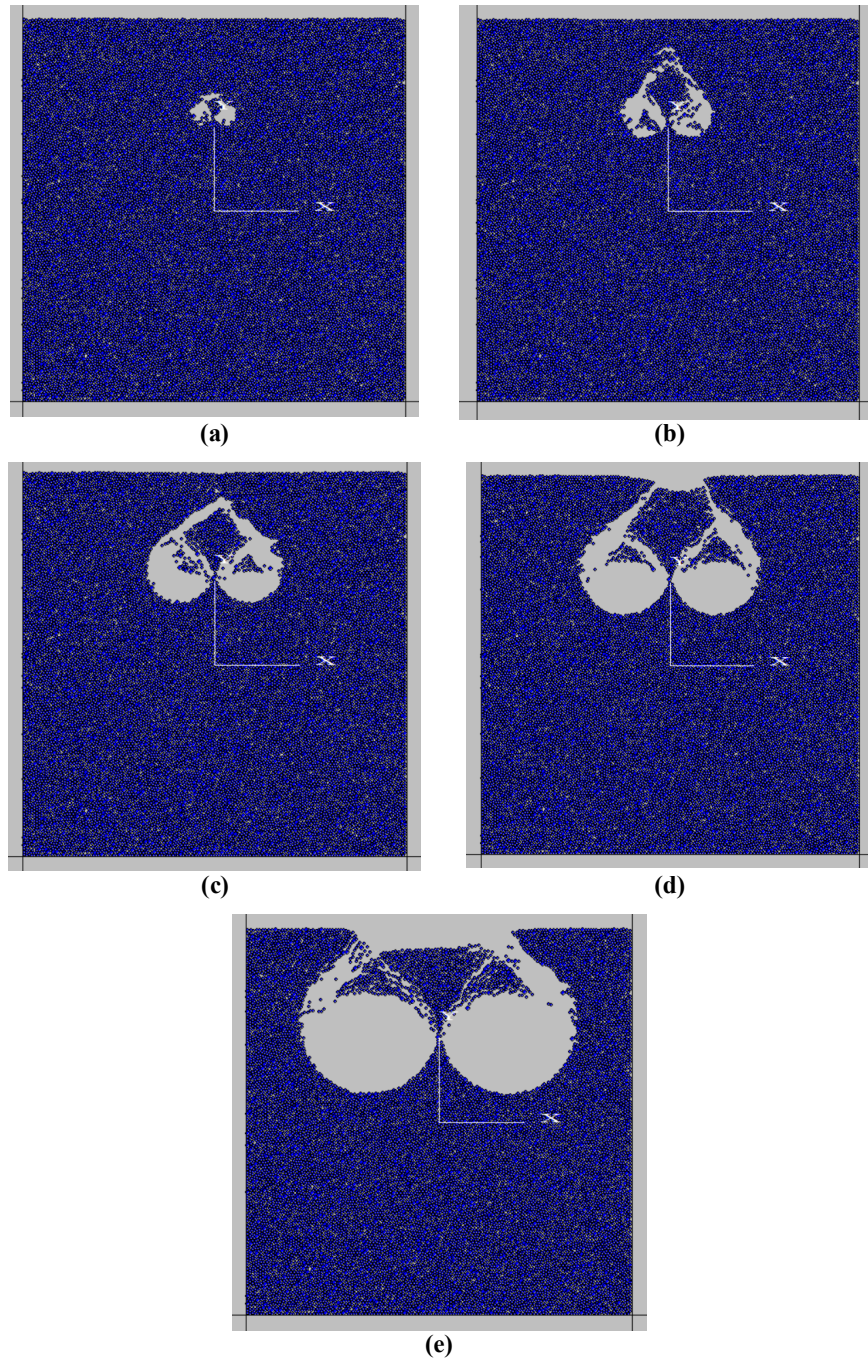


Figure 5. Collapse pattern in twin tunnel with diameters of a) 10 m, b) 15 m, c) 20 m, d) 25 m, e) 30 m.

### 3.3. Influence of single tunnel diameter on ground settlement above tunnel roof

Figure 6 depicts the influence of tunnel diameter on the ground settlement above the tunnel roof. The ground settlement was incremented by incrementing the tunnel diameter.

### 3.4. Influence of twin tunnel diameter on ground settlement above tunnel roof

Figure 7 depicts the influence of the twin tunnel diameter on the ground settlement above the tunnel

roof. The ground settlement was incremented by incrementing the tunnel diameter. By comparing Figure 6 and Figure 7, it could be concluded that

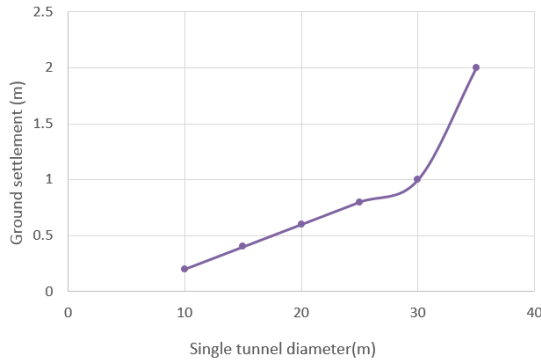


Figure 6. Influence of single tunnel diameter on ground settlement above tunnel roof.

the ground settlement was incremented by incrementing the tunnel number.

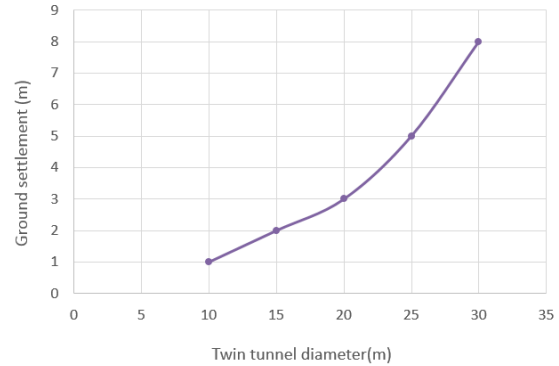


Figure 7. Influence of twin tunnel diameter on ground settlement above tunnel roof.

**3.5. Sensitivity analysis of collapse scope to examine effect of various micro-parameters such as contact bond normal strength, shear bond normal strength, particle friction coefficient, and stiffness ratio (kn/ks) on shape of single tunnel roof collapse**

Figure 8 depicts the failure mechanism of tunnel roof with regard to density = 2600 kg/m<sup>3</sup>, porosity = 0.08, contact young modulus = 1 GPa, and

confining pressure = 0.01 MPa. According to Figure 8a, it can be concluded that the widths of the collapse zone tend to decline as the parameter contact bond normal strength increases. Figure 8b depicts that the widths of the collapse zone tend to decline as the parameter contact bond shear strength increases. From Figure 8c and Figure 8d, it is clear that the failure zone is constant with increase in both the particle friction coefficient and the stiffness ratio.

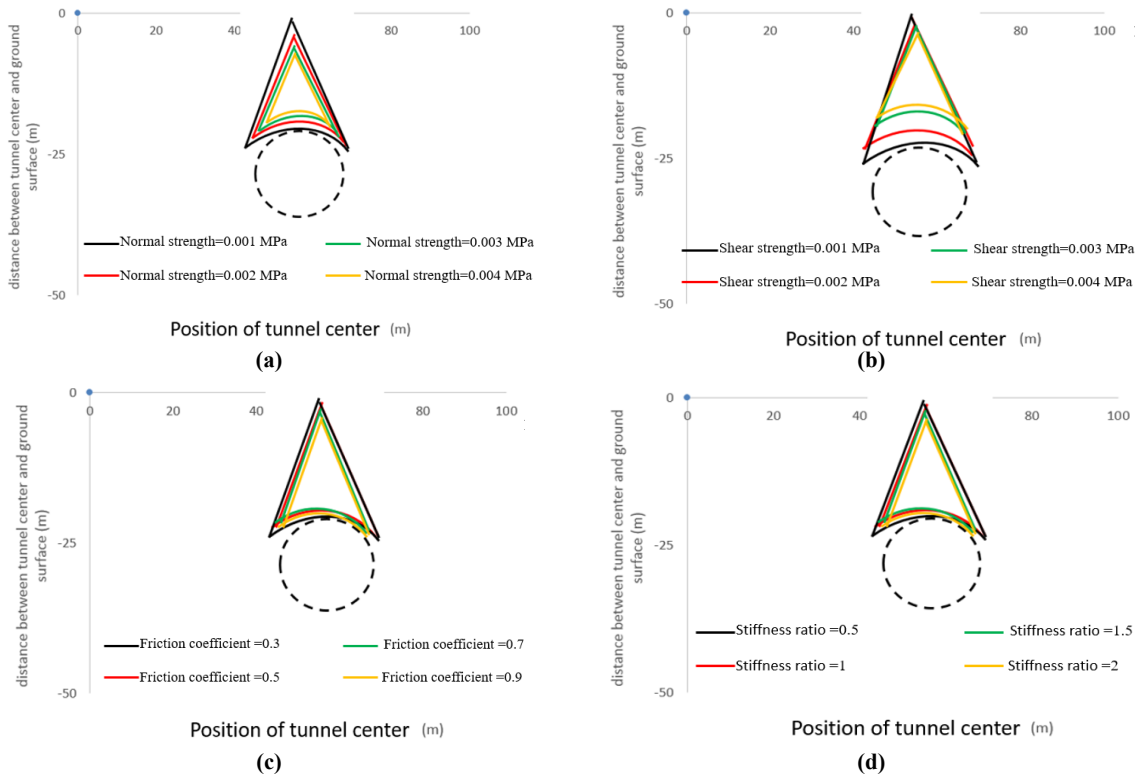


Figure 8. Influence of various factors on failure mechanisms of single tunnels: (a) Influence of contact bond normal strength on failure mechanisms, (b) Influence of shear bond normal strength on failure mechanisms, (c)

### Influence of particle friction coefficient on failure mechanisms, (d) Influences of stiffness ratio (kn/ks) on failure mechanisms.

### 3.6. Sensitivity analysis of collapse scope to explore influence of different micro-parameters such as contact bond normal strength, shear bond normal strength, particle friction coefficient, and stiffness ratio (kn/ks) on shape of twin tunnel roof collapse

Figure 9 depicts the failure mechanism of the tunnel roof with regard to density = 2600 kg/m<sup>3</sup>, porosity = 0.08, contact young modulus = 1 GPa,

and confining pressure = 0.01 MPa. According to Figure 9a, the widths of the collapse zone tend to decline as the parameter contact bond normal strength increases. Figure 9b depicts that the widths of the collapse zone tend to decline as the parameter contact bond shear strength increases. From Figure 9c and Figure 9d, it is clear that the failure zone is constant by increasing both the particle friction coefficient and the stiffness ratio.

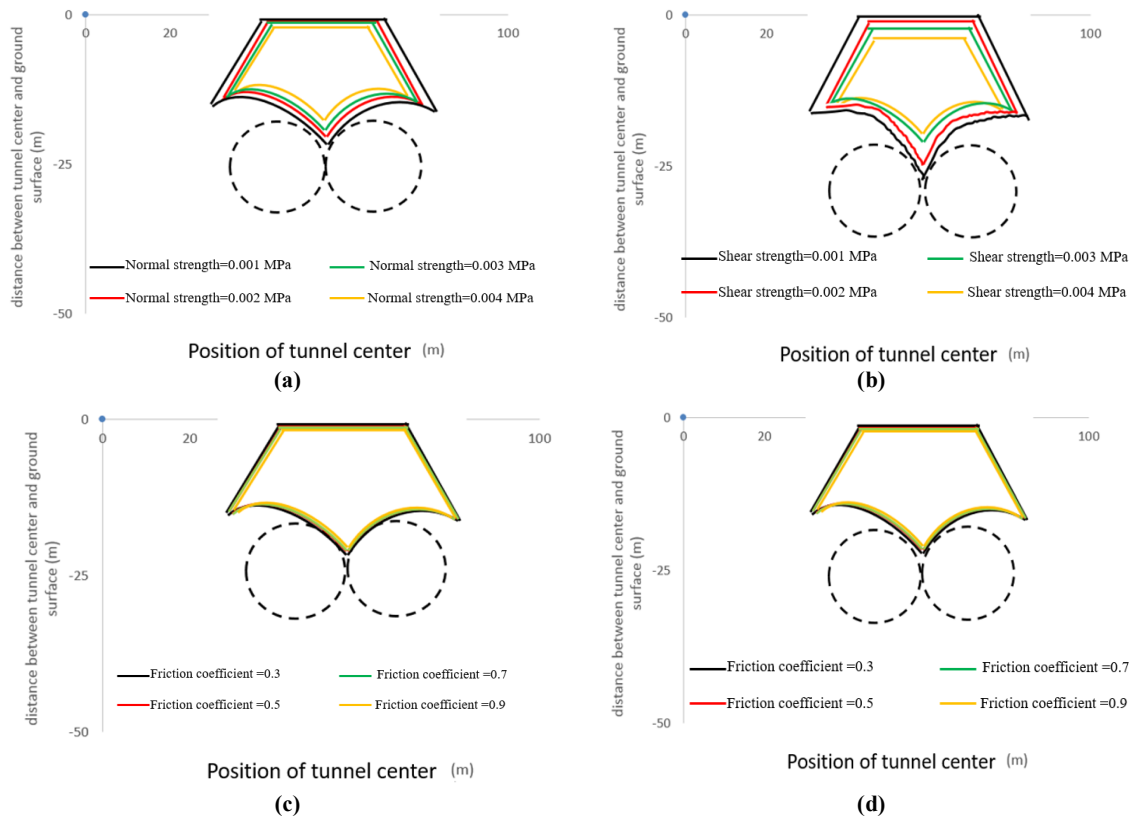


**Figure 9. Influence of various factors on failure mechanisms of single tunnels: (a) Influence of contact bond normal strength on failure mechanisms, (b) Influence of shear bond normal strength on failure mechanisms, (c) Influence of particle friction coefficient on failure mechanisms, (d) Influence of stiffness ratio (kn/ks) on failure mechanisms.**

## 4. Conclusions

In this investigation, the influence of single tunnel and twin tunnel on the collapse pattern and maximum ground movement was examined by particle flow code in two dimensions (PFC2D). Since first PFC was calibrated by the experiments, the test results were rendered by the uniaxial test. Further, a rectangular model with dimensions of 10 m \* 10 m containing both the central tunnel and the twin tunnel was built. The center of single tunnel was placed 25 m under the ground surface, and its

diameter was changed from 10 m to 35 m with an increment of 5 m. The center of the twin tunnel was placed 25 m under the ground surface, and their diameters were change from 10 m to 30 m with an increment of 5 m. A confining pressure of 0.01 MPa was applied to the model. The results obtained showed that:

- The volume of the collapsed wedge was incremented by incrementing the tunnel diameter.

- The volume of the collapsed wedge was incremented by incrementing the tunnel number.
- The ground settlement was incremented by incrementing the tunnel diameter.
- The ground settlement was incremented by incrementing the tunnel number.
- The widths of the collapse zone tend to decline as the parameter contact bond normal strength increases.
- The widths of the collapse zone tend to decline as the parameter contact bond shear strength increases.
- The failure zone was constant by increasing both the particle friction coefficient and the stiffness ratio.
- The failure zone volume was incremented by increasing the tunnel diameter.
- The failure zone volume was incremented by increasing the tunnel number.

## References

- [1]. Peck, R.B. (1969). Deep excavation and tunneling in soft ground. In: State of the art report, 7<sup>th</sup> international conference on soil mechanics and foundation engineering, Mexico City, pp. 225-290.
- [2]. Mair, R.J., Taylor, R.N., and Bracegirdle A. (1993). Subsurface settlement profiles above tunnels in clay, *Geotechnique*. 43 (2): 315-320.
- [3]. Cording, E.J. and Hansmire, W.H. (1975). Displacement around soft ground tunnels. In: Proceedings of the Pan-American Conference of Soil Mechanics and Foundation Engineering, 4: 571-663.
- [4]. Loganathan, N. and Poulos, H.G. (1998). Analytical prediction for tunneling-induced ground movements in clays. *J. Geotech. Geoenviron. Eng.* 124 (9): 846-856.
- [5]. Bobet, A. (2001). Analytical solution for shallow tunnels in saturated ground. *J. Eng. Mech.* 127 (12): 1258-1266.
- [6]. Rowe, R.K., Lo, K.Y. Kack G.J. (1983). A method of estimating surface settlement above tunnels constructed in soft ground. *Can. Geotech. J.* 20: 11-22.
- [7]. Addenbrooke, T.I. (1996). Numerical modelling in Stiff clay. PhD Thesis, Imperial College, London, UK.
- [8]. Franzius, J.N., Potts, D.M., and Burland, J.B. (2005). The influence of soil anisotropy and  $k_0$  on ground surface movements resulting from tunnel excavation. *Geotechnique*. 55 (3): 189-199.
- [9]. Zhao, Y. and Zhang, Y. (2019). Fracture behaviors of Tunnel lining caused by multi-factors: A case study. *Advances in Concrete Construction, An Int'l Journal* 8 (4):22-33.
- [10]. Jain, P. and Chakraborty, T. (2018). Numerical analysis of Tunnel in rock with basalt fiber reinforced concrete lining subjected to internal blast load. *Geomechanics and Engineering, An Int'l Journal*. 4 (1):56-76.
- [11]. Thai, D. and Nguyen, D. (2021). Safety assessment of an underground Tunnel subjected to missile impact using numerical simulations. *Computers and Concrete, An Int'l Journal*. 27 (1):87-98.
- [12]. Zhang, J. and Li, S. (2017a). Grouting influences evaluation of water-rich faults and its engineering application in Qingdao Jiaozhou Bay Subsea Tunnel, China. *Geomechanics and Engineering, An Int'l Journal*. 12 (1):98-111.
- [13]. Li Y. (2017) Model test and numerical simulation on the bearing mechanism of Tunnel -type anchorage. *Geomechanics and Engineering, An Int'l Journal, Vol.* 12 (1):111-121.
- [14]. Ding Z., (2017). Prediction methods on Tunnel -excavation induced surface settlement around adjacent building. *Geomechanics and Engineering, An Int'l Journal*. 12(2):45-56.
- [15]. Yang, X.L. and Li, W.T. (2017a). Reliability analysis of shallow Tunnel with surface settlement. *Geomechanics and Engineering, An Int'l Journal*. 12 (2): 33-44.
- [16]. Zheng, G. (2017). Characteristics and prediction methods for Tunnel deformations induced by excavations. *Geomechanics and Engineering, An Int'l Journal*. 12 (3):99-111.
- [17]. Yang, X.L. and Zhang R. (2017b). Collapse analysis of shallow Tunnel subjected to seepage in layered soils considering joined influences of settlement and dilation. *Geomechanics and Engineering, An Int'l Journal*. 13 (2): 86-98.
- [18]. Zhang, B., Wang X., Zhang J.S., and Meng F. (2017b). Three-dimensional limit analysis of seismic stability of Tunnel faces with quasi-static method. *Geomechanics and Engineering, An Int'l Journal* 13 (2):23-34.
- [19]. Aalianvari, A. (2017). Combination of engineering geological data and numerical modeling results to classify the Tunnel route based on the groundwater seepage. *Geomechanics and Engineering, An Int'l Journal*. 13 (4): 67-78.
- [20]. Mair, R.J. (1979). Centrifugal modelling of tunnel construction in soft clay. PhD Thesis, Cambridge University, Cambridge, UK.
- [21]. Taylor, R.N. (1984). Ground movements associated with tunnels and trenches. PhD Thesis, Cambridge University, Cambridge, UK.

- [22] Cooper, M.L., Chapman, D.N., Rogers, C.D.F. and Chan, A.H.C. (2002). Movements of the Piccadilly line tunnels due to the Heathrow express construction. *Geotechnique* 52 (4): 243-257.
- [23]. Suwansawat, S. and Einstein, H.H. (2007). Describing settlement troughs over twin tunnels using a superposition technique. *J.Geotech. Geoenviron. Eng.* 133 (4), 445-468.
- [24] Addenbrooke, T.I. and Potts, D.M. (2001). Twin tunnel interaction surface and subsurface influences. *Int. J. Geomech.* 1, 249-271.
- [25]. Hunt, D.V.L. (2005). Predicting the ground movements above twin tunnels constructed in London clay. PhD Thesis, University of Birmingham.
- [26]. Zhou, L. (2018). The influence of radial cracks on Tunnel stability. *Geomechanics and Engineering, An Int'l Journal.* 15(2): 59-67.
- [27]. Zou, J. (2017). Influences of seepage force and out-of-plane stress on cavity contracting and Tunnel opening. *Geomechanics and Engineering, An Int'l Journal.* 13 (6):111-121.
- [28] Chen, G. (2019) an improved collapse analysis mechanism for the face stability of shield Tunnel in layered soils. *Geomechanics and Engineering, An Int'l Journal.* 17 (1): 99-111.
- [29]. Zhang, R. and Yang, X.L. (2019). New 3D failure analysis of water-filled karst cave beneath dee Tunnel. *Geomechanics and Engineering, An Int'l Journal.* 18 (1): 46-57.
- [30]. Eftekhari, E. (2019). An overview of several techniques employed to overcome squeezing in mechanized Tunnel; A case study. *Geomechanics and Engineering, An Int'l Journal* 18 (2):87-99.
- [31]. Li, T.Z. and Yang, X.L. (2019). Face stability analysis of rock Tunnel under water table using Hoek-Brown failure criterion. *Geomechanics and Engineering, An Int'l Journal* 18 (3): 53-66.
- [32]. Gao, W. (2019). Prediction model of service life for Tunnel structures in carbonation environments by genetic programming. *Geomechanics and Engineering, An Int'l Journal* 18 (4):77-88.
- [33]. Li, T.Z. and Yang, X.L. (2019). Probabilistic analysis for face stability of Tunnel in Hoek-Brown media. *Geomechanics and Engineering, An Int'l Journal.* 18 (6):99-111.
- [34]. Sun, Q., Bo J., and Dias D. (2019). Viscous damping influences on the seismic elastic response of Tunnel in three sites. . 18 (6): 51-63.
- [35]. Wu, K. (2019). Mechanical analysis of Tunnel supported by yieldable steel ribs in rheological rocks. *Geomechanics and Engineering, An Int'l Journal.* 19 (1): 121-132.
- [36]. Lee, K. (2019). Electrical resistivity tomography survey for prediction of anomaly in mechanize Tunnel. *Geomechanics and Engineering, An Int'l Journal.* 19 (1): 176-188.
- [37]. Wang, L. (2019). Elastic solutions for shallow Tunnel excavated under non-axisymmetric displacement boundary conditions on a vertical surface. *Geomechanics and Engineering, An Int'l Journal.* 19 (3):187-196.
- [38]. Xue, Y. (2019). Stability evaluation for the excavation face of shield Tunnel across the Yangtze River by multi-factor analysis. *Geomechanics and Engineering, An Int'l Journal .* 19 (3):145-161.
- [39]. Wang, X. and Tian, L. (2018). Mechanical characteristics of coal-rock under different fracture-holes conditions: A numerical study based on particle flow code. *Environmental Earth Sciences.* 77 (8): 297.
- [40]. Wang, W, Wu, N. Li, H. and Yan, Y. (2020). Influence of joint angle on the instability failure characteristics and AE evolution law of underground caverns, *European Journal of Environmental and Civil Engineering.*
- [41] Chapman, D.N., Ahn, S.K., Hunt, D.V.L., and Chan, A.H.C. (2006). The use of model tests to investigate the ground displacements associated with multiple tunnel construction in soil. *Tunn. Undergr. Space Technol.* 21 (3-4), 413.
- [42] Chapman, D.N., Ahn, S.K., and Hunt, D.V.L. (2007). Investigating ground movements caused by the construction of multiple tunnels in soft ground using laboratory model tests. *Can. Geotech. J.* 44,631-643.
- [43]. Divall, S. (2013). Ground movements associated with twin-tunnel construction in clay. PhD Thesis, City University Londn, UK.
- [44]. Itasca Consulting Group Inc (1999). Particle flow code in 2-dimensions (PFC2D), Version 3.10.
- [45]. Potyondy, DO. and Cundall, PA. (2004). A bonded-particle model for rock. *Int J Rock Mech Min Sci* 41 (8): 1329-1364.

## تأثیر تونل‌های تک گانه و دوگانه بر الگوی ریزش و نشست سطح زمین

وهاب سرفرازی<sup>۱\*</sup>، کاوه عسکری<sup>۲</sup>

۱- بخش مهندسی معدن، دانشگاه صنعتی همدان، همدان، ایران

۲- بخش مهندسی معدن، دانشگاه شهید باهنر کرمان، کرمان، ایران

ارسال ۲۰۲۱/۰۸/۱۱، پذیرش ۲۰۲۱/۰۹/۰۷

\* نویسنده مسئول مکاتبات: Sarfarazi@hut.ac.ir

## چکیده:

به منظور بررسی تأثیر تونل‌های تک گانه و دو گانه بر الگوی ریزش و بیشینه جابجایی سطح زمین، از کد جریان ذره استفاده شد. در مرحله اول، نرم افزار PFC با نتایج تک محوره تست آزمایشگاهی کالیبره گردید. در مرحله دوم مدل‌های عددی با ابعاد  $100\text{ m} \times 100\text{ m}$  حاوی یک تونل و دو تونل ساخته شد. مرکز تونل‌ها  $25\text{ m}$  زیر سطح زمین است. قطر تونل تک گانه از  $10\text{ m}$  تا  $35\text{ m}$  با گام‌های  $5\text{ m}$  متغیر است. قطر تونل دو گانه از  $10\text{ m}$  تا  $30\text{ m}$  با گام‌های  $5\text{ m}$  متغیر است. برای اندازه گیری جابجایی عمودی، یک دایره اندازه گیر جابجایی با قطر  $2\text{ m}$  در سطح زمین بالای تاج تونل نصب شد. میانگین جابجایی عمودی دیسک‌های موجود در این دایره به عنوان نشست زمین در نظر گرفته شد. فشار محصور کننده  $0/01\text{ MPa}$  به مدل اعمال شد. گفتنی است که مقاومت تک محوره مدل  $0/09\text{ MPa}$  است. نتایج نشان دادند که قطر تونل کنترل کننده وسعت ناحیه آوار است. همچنین جابجایی قائم سقف تونل با کاهش قطر تونل، کاهش می‌یابد. نشست زمین با افزایش قطر تونل زیاد می‌شود.

کلمات کلیدی: تونل، PFC2D، نشست.